Mechanical Characterization of the Thoracic Ascending Aorta

Aaron Romo, Stéphane Avril, Pierre Badel, Jérôme Molimard, Ambroise Duprey, Jean-Pierre Favre

Abstract In this study the digital image correlation technique is used for characterizing the mechanical and rupture properties of aneurysmal tissues. The tissues which have been taken from the thoracic ascending aorta of diseased patients are tested in a bulge inflation test. The approach is original in the sense that it gives access to the local stress fields in the tissue and to local analysis of rupture. Applications to the dynamic behavior and rupture of vascular tissues are envisaged.

Keywords aneurysm, human aorta, inflation test, rupture, ultimate stress.

I. INTRODUCTION

Cardiovascular diseases represent a major public health issue in the industrialized countries. According to the World Health Organization (W.H.O.) cardiovascular diseases are the first cause of death in the world [1]. Cardiovascular diseases include many disorders affecting the heart and blood vessels. The most frequent are atherosclerosis and cerebrovascular accidents (CVA) but also include other kinds of arterial wall pathologies like dissections or aneurysms which can cause the death of 60 000 people every year in the industrialized world if not treated. Aortic aneurysms alone are the 13th cause of death in the industrialized world [2]-[3].

Aortic ruptures may occur spontaneously, after a pathological condition like aneurysms or dissections, and sometimes after traumatic events like motor vehicle accidents.

Motor vehicle accidents frequently lead to non-penetrating thoracic aortic injuries, which are highly lethal. In 80-90% of the cases of thoracic aortic injury, patients will die within the first hours [4]-[5] and approximately 2% of surviving patients will not be diagnosed initially with aortic injury and will develop chronic pseudoaneurysms which can, eventually, rupture [5]-[6]. In such accidents, aortic injuries are caused mainly by horizontal decelerations at different attachment sites of the thoracic aorta. Particularly in the proximal part of the aorta, the deceleration event will provoke the lengthening of the ascending aorta and the torsion of the aortic root caused by the displacement of the heart into the left pleural cavity [7]-[8].

Another important factor determining the aortic injury is the sudden increase of the aortic intraluminal pressure. Oppenheim [9] found that the ascending aorta in cadavers ruptured when a pressure of approximately 3000 mmHg was suddenly applied within the aorta [8]. This was one of the first times that the human aortic tissue was pushed to its limits in order to describe its behavior.

Since then, mechanical tests have been the most common way to characterize the mechanical behavior of aortic tissue and to predict its rupture. For example Okamoto et al. [10] used planar biaxal stretching tests, uniaxial strength tests and opening angle methods to measure elastic properties, strength, and residual stress in dilated thoracic ascending aorta.

Choudhury et al [11] used biaxal tensile tests to compare different regions of the human thoracic ascending aorta in pathological and healthy conditions. They found different properties between regions but these properties were not directionally dependent, suggesting that pathological tissue is isotropic, while healthy tissue is rather anisotropic.

Using mechanical testing approaches allow enlarging the possible use of other approaches like mathematical modeling. In this concern, different authors have tried to model healthy and pathological arterial behavior by

Aaron Romo is a PhD student in Biomechanics at Ecole National Superieure des Mines de Saint Etienne (ENSMSE) (+33 (0)4 77 42 93 29, romo@emse.fr). Stéphane Avril is Professor of Biomechanics and Director of the Center for Health Engineering at ENSMSE. Pierre Badel is Assistant Professor at ENSMSE. Jérôme Molimard is Professor at ENSMSE. Ambroise Duprey is a Vascular Surgeon (MD) at the Cardiovascular Surgery Service of the University Hospital Center Hôpital Nord. Jean-Pierre Favre is Professor and Vascular Surgeon (MD, PhD) at the Cardiovascular Surgery Service of the University Hospital Center Hôpital Nord.

conceiving their own constitutive equations [12]-[16]. These physical relations can approximate the response of material to external stimuli. In these equations material constants have to be determined by mechanical tests and the parameters of the equations are fitted to the test results.

Mechanical approaches to characterize aortic aneurysms are still in early stages, even if a lot of progress has been made, today there is still no consideration of mechanical criteria in standard surgical treatments. The main and almost the only criterion used to operate thoracic ascending aneurysms is when the aneurysm reaches a diameter of 55 mm [3], [17]-[18].

Even though there is a general consensus in the surgical interventional criterion of 55 mm, it is still very debatable. According to Nicholls et al. [19] and Pape et al. [20] it has been shown that aneurysms below the interventional criterion of 55 mm can rupture or dissect, leading to the controversy of whether small aortic aneurysms should be repaired or not. The International Registry of Aortic Dissection (IRAD) noted the same phenomenon [20], but recognized the dangers of reducing size criterion for surgical intervention. This would mean that many more people could be affected by this measure and there might be more harm caused by operating on small sized aneurysms rather than leaving the criterion unchanged [21].

Furthermore, the diameter size criterion does not consider the shape of the aneurysm which could be important. On this regard, Vorp et al. [22] determined the distribution of mechanical wall stress into an abdominal aortic computational model, finding that the shape of the aneurysm is as important as the maximum diameter of the aneurysm in order to determinate the maximum stress distribution and possibly the rupture of the aneurysm.

These are the main reasons why mechanical criteria should be introduced when evaluating the risk of rupture or dissection of the thoracic aortic wall. To this objective, the development of accurate experimental procedures and the acquisition of more experimental data are required. The experimental procedure introduced in this paper consists of an inflation test performed on circular patches of fresh aneurysmal tissue, linked to strain measurements by digital image stereo-correlation. The purpose of this work is first of all to create a database providing detailed and accurate mechanical characterization of aneurysmal tissue rupture in order to better understand the phenomenon of the aneurysm rupture. It will eventually lead to creating new intervention criteria based on the mechanics of aortic tissue rather than just the diameter size of the aneurysm.

II. METHODS

The experimental inflation test consists of injecting water into a hermetically sealed cavity, formed by the aortic tissue and the inflation test device, provoking the deformation of the tissue as the water is filling the cavity. Using Digital Image Stereo-Correlation System (DIS-C) the 3D shape of the inflated aortic specimen can be recreated in order to calculate its radius of curvature. Full-field strain measurements also obtained by DIS-C will be used to calculate the strains and final thickness during the inflation. Finally, the rupture stress of the aortic specimen will be evaluated using the Laplace's law.

Materials

The experimental procedure is conducted using aneurysmal aortic specimens from patients who required a surgical replacement of the pathological segment of the ascending aorta. An agreement has been established with the University Hospital Center of Saint Etienne in order to have access to those specimens, following the guidelines of the local Institutional Review Board.

A total of 11 different aneurysmal aortic tissues are used for the experimental procedure leading to 15 valid specimens for experimental tests (Table 1). Specimens are kept in refrigeration at +4°C in a 0.9% physiological saline solution. Tests are performed within 24 hours after excision which let us make the hypothesis that the mechanical properties of the tissue are maintained in this period of time [23]. During the entire experimental procedure we try to maintain the specimen layer as well irrigated as possible in order to preserve its mechanical properties.

TABLE 1. Demographic information of the specimens

Test no.	Layer Type	Sex/Age	Diameter before surgery (mm)	Initial Thickness (mm)
1	adventitia	M/67	50	1.18
2	adventitia	M/36	50	0.51
3	adventitia	M/55	53	0.79
4	adventitia	M/81	54	0.64
5	adventitia	M/76	52	0.62
6	adventitia	M/71	48	0.55
7	media	M/70	63	0.89
8	media	M/67	50	0.68
9	media	M/54	60	0.98
10	media	M/55	53	1.09
11	media	F/76	55	1.15
12	media	M/81	54	0.91
13	media	M/68	59	1.02
14	media	M/69	51	1.09
15	media	M/71	48	1.04

The cylindrical aortic specimen (Fig. 1-I) is cut in the axial direction, which is the blood flow direction, and then the specimen is laid flat in order to evaluate the best area for the test to be performed. Specimen areas presenting pathological calcifications or intimal thrombosis are discarded from the study. The residual stress in the aortic specimens during the experimental procedure is not considered in this study because flat positioning of the opened section of the cylindrical vessel is assumed to be stress-free [24]. Large-sized aortic specimens allow performing two experimental procedures, even though it is rare. Inversely, sometimes, the specimen is so small that no experimental procedures can be performed.

The next step consists of cutting a square flat piece of the specimen of approximately 45mm x 45 mm. From the square flat specimen we remove very carefully, using dissecting blunt-point scissors, the loose connective tissue which is attached to the adventitia layer (Fig. 1-II). This tissue is removed because it is of no interest from the mechanical point of view in this study and also because it will make the specimen slide during the inflation test.

The remaining square specimen contains the tunica intima, media and adventitia. It was decided to separate the square specimen into two layers, the intima-media and the adventitia. The inflation test will be performed with each of the layers, allowing two different tests by aortic specimen if all conditions are satisfied. Mechanically, the two more important layers are the tunica media and the adventitia in healthy arteries [24]. Different mechanical properties can be found on each of these two layers, which is the reason why we test them separately. In this study, the mechanical contribution of the tunica intima is neglected, or more precisely it is considered to be part of the tunica media.

The separation between the two layers is accomplished by differentiating the color of each layer; the media being yellowish while the adventitia being pinkish. A starting incision is made with the dissecting scalpel in the transition zone between the tunica media and adventitia (Fig. 1-III). We can finally separate them by pulling each layer very carefully trying to reduce the damage on the surface. The square pieces will be marked in the upper right corner (Fig. 1-IV) distinguishing the axial and circumferential directions which is important to characterize the rupture orientation angle.

The average thickness of each layer was measured at zero stress state using a digital caliper, putting the layer of interest between two plates so as to homogenize the measured surface.

Inflation Test

The inflation test has been chosen in order to identify the radius of curvature and the rupture stress parameters. The advantage of this kind of test is that it will reproduce in vivo pressurized conditions. In our

case, water under pressure will be used to generate biaxal stress states in the specimen.

First, the layer of interest is positioned into the inflation test device (Fig. 1-V) matching the axial direction of the specimen layer with the vertical direction in the device, and the circumferential direction with the horizontal one. The axial direction is the one which follows the blood flow direction and the circumferential direction is perpendicular to the axial direction.

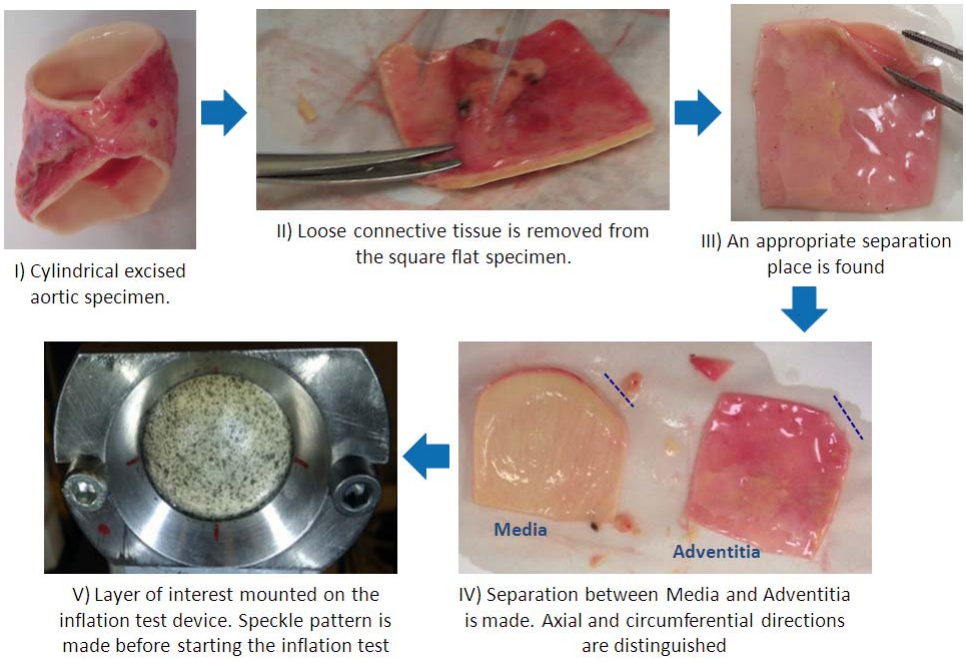

Fig. 1 Experimental procedure: from aortic specimen preparation to the inflation test

The layer of interest is maintained flat and tightened between the two parts of the inflation test device: the injecting face which is the side of the device that will introduce the water under pressure into the cavity and the holder face of the device that is basically a rectangular plate with a circular hole in the middle permitting the outwards inflation of the tissue through it. Also the holder face will maintain a hermetically sealed cavity. Both of these parts of the device, together with the tissue to be tested, are held by two screws that we can adjust depending on the thickness of the layer of interest.

The creation of the speckle pattern on the luminal side of the layer is made once the layer of interest is set on the inflation test device (Fig. 1-V). The speckle pattern is a random spread of paint, homogeneous all over the surface. The technique consists in laying the surface horizontal and spraying in the air slightly above the surface. The surface is then marked indirectly by small drops of paint falling on it and forming the pattern. It is important to maintain the same distance from the surface and the same opening on the valve of the spray paint during the painting in order to obtain a regular drop size. The speckle pattern will be fixed to the surface during the deformation process caused by the inflation test (Fig. 1-V); consequently the speckle pattern's deformation will represent the surface deformation towards the DIS-C system. Note that the luminal side of each layer is chosen to be painted because it is the side where the surface and color of the tissue is more uniform. This aspect is important for improving the quality of the speckle pattern. Using the external side of the layer with the inflation test would have more resemblance to what actually happens during the dilation of an aneurysm in vivo. The problem is that the external side is highly irregular and viscous making difficult the speckle pattern to adhere to the surface.

In addition, components of the spray paint affecting the specimen's mechanical properties of the layer will be neglected [25].

The execution of the test consists of injecting water at a constant rate by pushing a piston pump at 15 mm/min until the tissue is ruptured. Simultaneously, the pressure is measured with a digital manometer connected to the piston pump. Before performing the inflation test, five successive pressurization cycles from 0

to 11 kPa are executed to achieve pre-conditioning.

The water under pressure into the hermetically sealed cavity provokes the deformation of the layer and consequently the deformation of the speckle pattern until the rupture. All the stages of the inflation are monitored with the DIS-C system, protected from bursting water by a transparent acrylic plate. Images are taken using the DIS-C system every 0.003 MPa, with an average total of 18 images taken for each test. A similar technique was proposed by Mohan and Melvin [26] which allowed determining one-dimensional elastic properties using two photographic cameras and uniaxial tensile tests instead of a DIS-C system and inflation tests.

Fig. 2 shows an overall view of the experimental set-up.

Digital Image Stereo-Correlation (DIS-C)

The DIS-C system used (including the Aramis® software) is a commercial system developed by GOM® [27], it is composed of two 8-bit CCD cameras, allowing 256 different gray levels and having a resolution of 1624 x 1236 pixels. Each camera is equipped with a 50mm lens, the incidence angle is about 27° and a laser pointer is placed between the two cameras to guide the measures.

To set up the DIS-C system, it is necessary to position the cameras, focus each of the cameras using the maximum aperture size in order to improve focusing. Right after finishing the focus, the aperture must be changed again to the minimum value with the purpose of increasing the depth of field during the image recording. Increasing the depth of field in the images will be critical because the inflation test is an out-of-plane displacement and it is important that the system is maintained in focus during the whole inflation process. Next, the polarizing filters must be adjusted to reduce noise effects, like excessive brightness or parasite reflections.

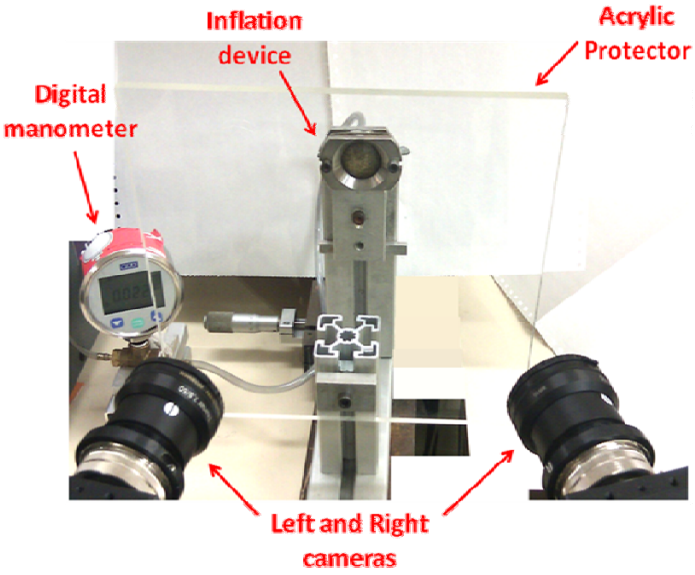

Fig. 2 Experimental set-up

The calibration of the DIS-C system is done with the help of an adequate calibration panel corresponding to our measured volume. The calibration ensures the dimensional coherence of the system. During this process the distance from the system to the specimen and the orientation of the cameras to each other is determined.

A lot of attention is paid to each of these steps because the accuracy of the procedure depends on the quality of the calibration.

Once the experimental procedure is finished, image processing is performed using Aramis® software.

From the images acquired (Fig. 3), the Area of Interest (AOI) is delimited on the first image. Here, the AOI is a circle measuring 30 mm diameter, excluding the rest of the image.

The following parameters are chosen for DIS-C processing. The facet size and the facet step are chosen as a function of the speckle pattern dot size, distribution and contrast (Fig. 4). These tests have a facet size of 21 pixels (px) and a facet step of 5 px, which means that we will divide the AOI from every image into small squares

of 21 x 21 px² with a 5 px overlapping area. The system will be allowed to identify different gray levels in all facets, making every facet distinguishable from each other. This will permit the facets to be tracked during the different load stages of the inflation test (Fig. 5).

Choosing a facet size of 21 px and a facet step of 5 px yields a resolution of 0.54 µm (0.02 px) for in-plane displacement and 1.5 µm for out-of-plane displacement.

The 3D surface will be created once the system will determine the 2D coordinates of the corner and the center of the facets (Fig. 6). Using a technique called stereophotogrammetry the 2D coordinates observed from the left camera and the same coordinates observed from the right camera will yield the 3D coordinates. The process is based on the mimic of the human stereoscopic vision.

As we are working under large deformations, it is necessary to set consecutive images as reference from one to another in order to find a correlation between them.

Fig. 3 View of the specimen during the inflation test through the left and right cameras from Aramis® software.

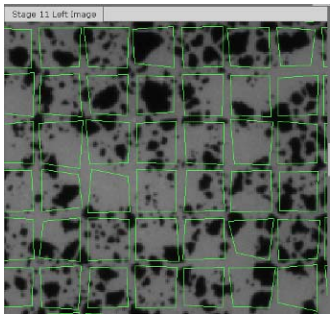

Fig. 4 Creation of the facet field in the Aramis® software. thanks to the speckle pattern

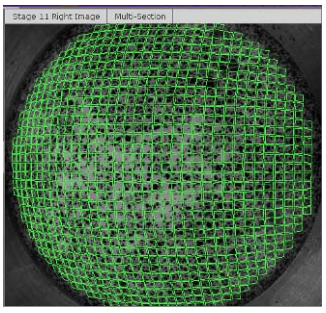

Fig. 5 Facet field distribution on the inflated specimen using Aramis® software.

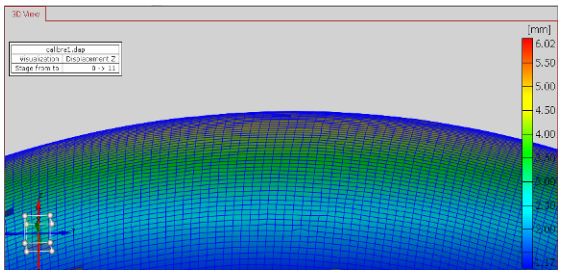

Fig. 6 Creation of a 3D surface using Aramis® software.

Rupture Stress Calculation

In order to calculate the rupture stress on the inflated layer, the proposed methodology consists of finding the radius of curvature of the inflated layer just before the rupture and in using Laplace's law to calculate the tension and the rupture stress of the inflated layer at rupture.

The first step consists in loading into Matlab® the coordinates of all the points to form the 3D surface of the inflated layer just before rupture (Fig. 7). A semi-spherical geometry is then created and fitted onto the actual surface using an in-house Matlab® code. This process is represented in Fig. 8 where: (I) is the first loading data stage, (II) is the creation of the semi-spherical shape (green) just under the loaded data (blue) and (III) is the mixed representation of the loaded data (blue) and the fitted semi-spherical shape (red).

The aim of this process is to make a global analysis using the inflated specimen without the local fields, which can be obtained through the DIS-C system. Kim et al. [30] made a local analysis of an inflated specimen using stress fields and solving an inverse problem.

The advantage of approximating the semi-sphere to the 3D surface of the aortic specimen is to have an analytical representation of the surface. It is thereby possible to obtain the global radius of curvature.

This calculation is made all over the inflation process, but the final radius is taken from the last image just before the rupture of the inflated aortic layer.

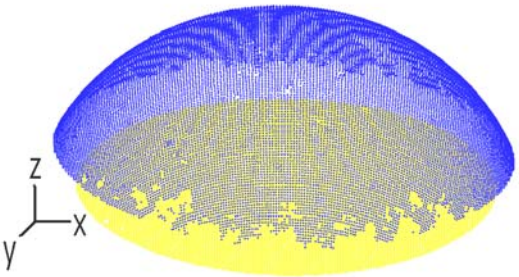

Fig. 7 The 3D reconstructed surface of the aortic specimen layer from the initial stage (yellow) to the final stage (blue) during the inflation test.

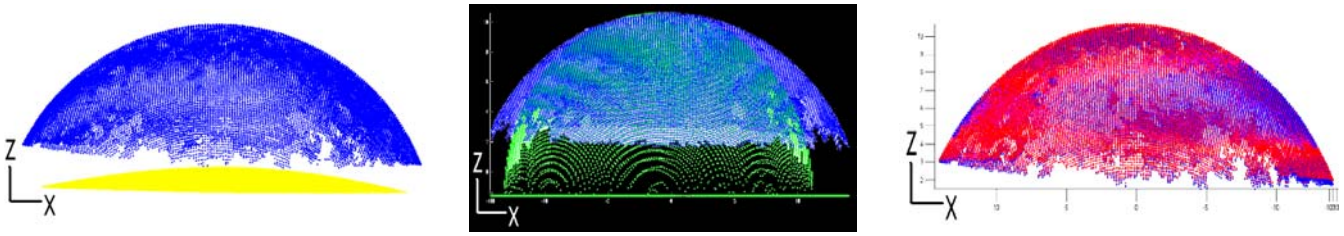

(I) (II) (III)

Fig. 8 Fitting process of the semi-spherical shape in green (II) into the reconstructed surface from the aortic specimen layer in blue. Final fitted semi-spherical shape is represented in red (III).

Rupture stress calculation also requires the input of the thickness of the specimen at rupture. Its calculation needs several steps to be achieved. Using Aramis® software through the DIS-C system, the membrane strain values are obtained at each stage by transforming the 3D data created before into the 2D space. In order to achieve this transformation, Aramis® software uses a method which projects perpendicularly the 3D data into a tangential plane, resulting in sets of points in the 2D space. The deformation gradient tensor $\underline{\underline{F}}$ from the 2D sets of points in the undeformed and deformed state can now be calculated in order to finally calculate the Green-Lagrange strain tensor $\underline{\underline{e}}$ in the local tangent frame.

$$\underline{\underline{e}} = \begin{pmatrix} \frac{1}{2}\left(\lambda_1^2 - 1\right) & 0 & 0 \\ 0 & \frac{1}{2}\left(\lambda_2^2 - 1\right) & 0 \\ 0 & 0 & \frac{1}{2}\left(\lambda_3^2 - 1\right) \end{pmatrix} \qquad (1)$$

where λ is the stretch ratio in different directions. In this formula the out-of-plane stretch ratio, λ_3 related to thickness changes remains unknown.

The calculation of the thickness change of the specimen during the inflation test is performed using the average Green-Lagrange strain values and the assumption of incompressibility ($\det(\underline{\underline{F}}) = 1$). The average strain values $\overline{E}_{xx}$ and $\overline{E}_{yy}$ are calculated from the results of the DIS-C analysis and incompressibility, yielding:

$$\lambda_3 = \frac{t_n}{t_o} = \frac{1}{\sqrt{2\overline{E}_{xx}+1}\sqrt{2\overline{E}_{yy}+1}} \qquad (2)$$

where λ_3 is the thickness ratio, t_o is the thickness at a zero stress state (mm), t_n is the thickness at the final stage (mm).

The last step towards rupture stress calculation involves the Laplace's law. This equation relates the surface tension to the pressure and the radius of curvature. In our case, it has the following form:

$$T = \frac{p \cdot r}{2} \qquad (3)$$

where T is the tension on the surface (N/mm), p is the pressure at final stage of the inflated specimen layer (MPa), and r is the radius of curvature calculated for the final stage (mm).

The stress at rupture is calculated using the final thickness t_n of the layer:

$$\sigma = \frac{p \cdot r}{2 \cdot t_n} \qquad (4)$$

where σ is the rupture stress calculated at the final stage of the inflated specimen layer (MPa), and t_n is the final thickness of the specimen layer (mm) obtained with Eq. (2).

Rupture Orientation Angle

The rupture orientation angle (Fig. 9) is calculated using the images obtained from the DIS-C system at the moment of the rupture or just after the rupture. A series of points are marked on the image following the rupture orientation exactly in the area of the rupture. A linear regression trend line is fitted using those points and the angle between this line and the circumferential direction (horizontal direction) is calculated.

The specimens for which the rupture did not initiate at the centre of the inflation device were discarded. Thanks to this precaution, it is assumed that the observed rupture in the specimens kept for further analysis is not affected by the boundary conditions.

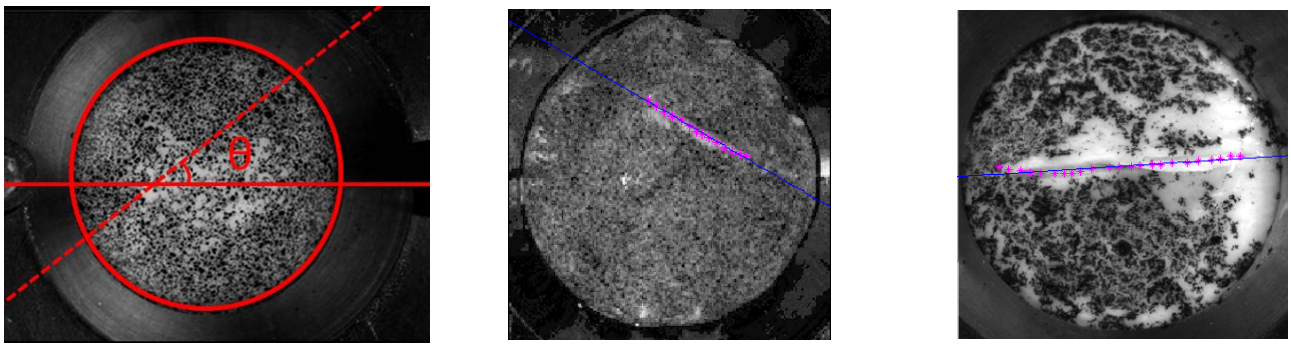

(a) (b) (c)

Fig. 9 Rupture orientation angle "θ" (a) is calculated with respect to the circumferential direction (horizontal). In (b) the angle obtained was 29.54°; in (c) it was 3.61°.

III. RESULTS

A total of 11 different aneurysmal aortic tissues were obtained through an agreement established with the University Hospital of Saint Etienne, France. Inflation experimental tests were carried out in 22 different specimen layers of those 11 aortic tissues. For this study only 15 specimens were taken into account because for the other specimens rupture did not occur in the center of the AOI during the inflation tests. Seven specimens were not included because rupture occurred at the boundaries, or because of other reasons making the data

useless. The results obtained are presented in Table 2.

From the total of 15 different specimens, 6 were adventitia layers and 9 were media layers. Only one specimen layer was from a female patient and the average age of the patients was 66 years old. From the beginning to the end of the inflation tests, media specimens were thicker than adventitia specimens. It is interesting to note the relationship between age of the patient and rupture stress. The youngest patient's specimen (test no. 2) had clearly the largest rupture stress (3.58 MPa) of all, although the oldest patient's specimen (test no. 12) was not the weakest (0.56 MPa).

TABLE 2. Results grouped by layer type

Test no.	Layer Type	Pressure at Rupture (MPa)	Radius of Curvature (mm)	Final Thickness (mm)	Tension (N/mm)	Rupture Stress (MPa)	Rupture Angle (°)
1	adventitia	0.066	17.70	0.60	0.5842	0.9695	22.79
2	adventitia	0.081	19.50	0.22	0.7802	3.5825	1.28
3	adventitia	0.053	17.19	0.39	0.4557	1.1725	73.29
4	adventitia	0.041	18.75	0.47	0.3846	0.8116	29.54
5	adventitia	0.062	18.44	0.36	0.5719	1.5928	23.58
6	adventitia	0.031	17.57	0.32	0.2725	0.8414	24.22
7	media	0.047	17.64	0.57	0.4147	0.7275	3.61
8	media	0.056	18.61	0.37	0.5211	1.4016	41.84
9	media	0.044	17.85	0.46	0.3927	0.8503	64.33
10	media	0.059	17.38	0.62	0.5127	0.8215	85.38
11	media	0.052	17.33	0.93	0.4853	0.4863	15.03
12	media	0.038	17.22	0.59	0.3273	0.5559	16.31
13	media	0.064	17.87	0.79	0.5720	0.7283	3.20
14	media	0.071	18.04	0.78	0.6405	0.8244	26.09
15	media	0.040	19.55	0.61	0.3911	0.6386	28.03

Radius of curvature calculated was always in the same range of values with the smallest being 17.19 mm (test no. 3) and the biggest 19.55 mm (test no. 15), which means that the average radius of curvature for all specimen layers was 18.04 mm (standard deviation: 0.77 mm). Radius of curvature values for each of the specimens are shown in Fig. 10-a. Two thirds of the media specimens contributed to this average value as shown in Fig. 10-b.

Rupture stress values for each of the specimens are shown in Fig. 11-a. The average rupture stress was 1.06 MPa (standard deviation: 0.46 MPa). 80% of specimens ruptured in this average value (see Fig. 11-b). Distinguishing adventitia and media specimens, the first had an average rupture stress value of 1.49 MPa (standard deviation: 1.06 MPa) and media specimens had an average value of 0.78 MPa (standard deviation: 0.26 MPa). On average, adventitia is thinner than media but it has larger rupture stresses.

Rupture angle values for each of the specimens are shown in Fig. 11-a. Rupture angle average for all specimen layers was 30.57° (standard deviation: 25.43°), where two thirds of media specimens and half of the adventitia specimens contributed to this average value as shown in Fig. 12-b. Adventitia specimens alone had an average rupture angle value of 29.12° (standard deviation: 23.75°) and media specimens had an average value of 31.54° (standard deviation: 27.86°).

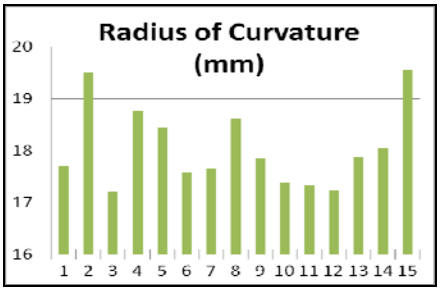

(a) number: test no.

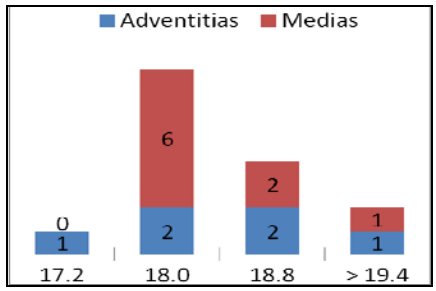

(b) Frequency distribution of adventitia and media in function of radius of curvature (mm).

Fig. 10

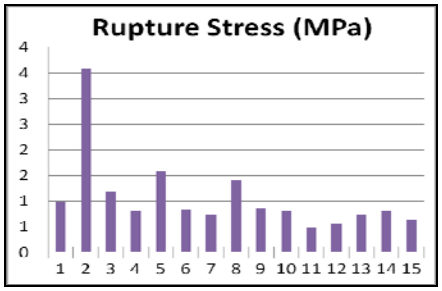

(a) number: test no.

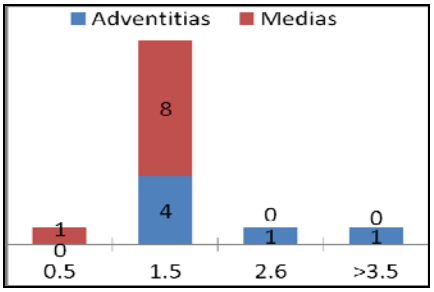

(b) Frequency distribution of adventitia and media in function of rupture stress (MPa).

Fig. 11

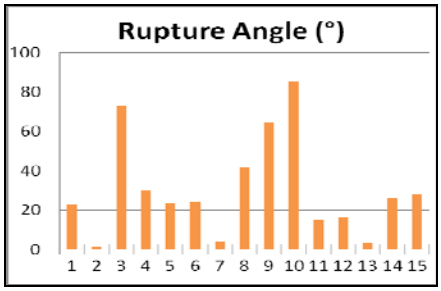

(a) number: test no.

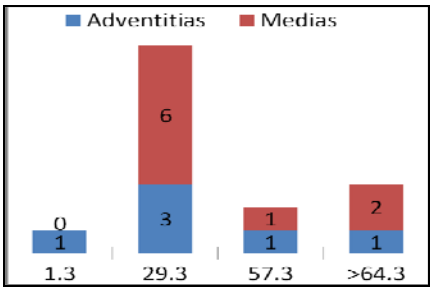

(b) Frequency distribution of adventitia and media in function of rupture angle (°).

Fig. 12

The behavior of the aortic specimen layers under loading conditions can be described using stress-strain curves as shown in Fig. 13. Measured Lagrange strain fields in the circumferential E_{xx} and axial E_{yy} directions, for every stage of the inflation test, show the non-linear behavior of the aortic specimens, as the load is supported by the progressive recruitment of collagen fibers.

Comparing the non-linear behavior in the circumferential and axial directions, it can be seen that they present almost the same maximum stress values for each of the specimens presented in Fig. 13, meaning that the aneurismal tissue has almost an isotropic behavior.

Performing uniaxial and equibiaxial tests some authors have found no directional dependence, describing the human ascending aorta as mainly isotropic [16], [28]. This is consistent with our results.

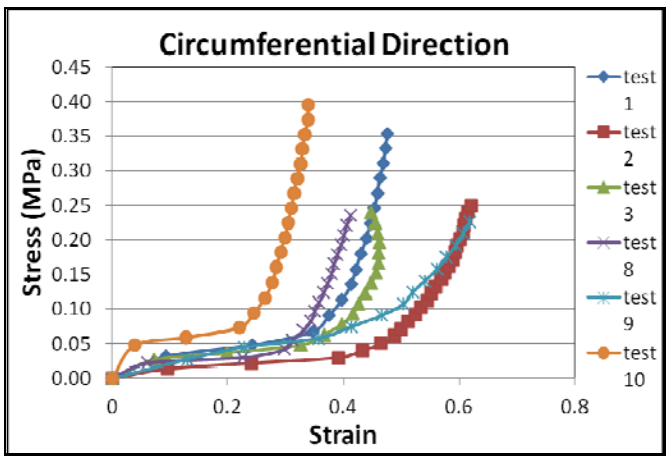

(a)

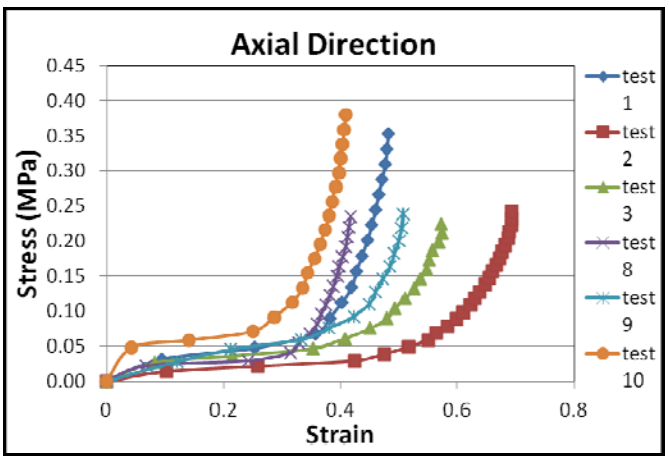

(b)

Fig. 13 Stress-strain curves for three adventitia specimens (test no. 1, 2, 3) and three media specimens (test no. 8, 9, 10) in the circumferential (a) and axial (b) direction.

IV. DISCUSSION

Using the DIS-C technique and a specific analysis, quantitative values of ultimate stresses have been reported

in biaxial inflation testing for aneurysmal tissue.

It has been shown that rupture occurs in preferred directions, indicating some anisotropy of the tissue. In this study the anisotropy is somehow marginal during the elastic deformation of the tissue as a semispherical shape fits well the deformed shape of the aortic specimen. The anisotropic elastic properties of the arteries were already characterized using a similar technique [29]-[30] and it already revealed that there was no clear trend regarding the preferred orientation of collagen fibers in the tissue. This was attributed to the effect of degenerative process in the diseased tissue [30].

However, it was observed here that rupture occurs in a preferred direction. The tear rupture was often preceded by a local weakening of the mechanical properties of the tissue, especially in the intima and media layers which are more fragile [30]. It would be interesting to improve the quality of the speckle pattern in order to improve the spatial resolution of the full-field measurements and therefore to characterize more finely the rupture mechanisms.

In the present study, only specimens which ruptured in the center of the AOI were taken into account. The inflation test is assumed to be under uniform biaxial loading at the center of the AOI. Therefore, the boundary conditions of the inflation device are assumed to have only a marginal impact on the observed rupture of the pieces of artery.

Effects of age were observed with the relatively large ultimate stress of the tissue coming from the youngest patient. However, no clear trend comes up from the rest of the data and other tests should be conducted for completing the database and achieving statistical analysis.

The properties of different locations of the aorta were not compared here as was done in the study of Haskett et al. [31]. However, differences of properties were highlighted between the tunica media and the adventitia. The latter is found stronger, which confirms its role of structural support of the artery [12].

V. CONCLUSIONS

Based on an original approach combining inflation tests and an imaging technique, this paper has presented one of the rare studies providing quantitative values of ultimate stresses in aortic aneurysms. It has potential application to understanding aortic injuries due to severe mechanical loading in car crashes. One of the potentials of this work is to be able to predict the probability of rupture in such circumstances. For this, dynamic conditions of loading will have to be developed in the currently existing protocol.

VI. ACKNOWLEDGEMENT

The authors would like to acknowledge the National Council on Science and Technology of Mexico (CONACYT) for funding Mr. Romo's scholarship.

VII. REFERENCES

[1] Mendis S, Puska P, Norrving B, World Health Organization, Global Atlas of Cardiovascular Diseases Prevention and Control, page 1, 2011.
[2] Isselbacher EM, Thoracic and Abdominal Aortic Aneurysms, Circulation, 111, 816-28, 2005.
[3] Nawwar A, Nataf P, Anévrismes de l'Aorte Thoracique Ascendante, La presse médicale, 39, 26-32, 2010.
[4] O'Connor JV, Byrne C, Scalea TM, Griffith BP, Neschis D, Vascular Injuries After Blunt Chest Trauma: Diagnosis and Management, Scandinavian journal of trauma, resuscitation and emergency medicine, 17, 42, 2009.
[5] Parmley LF, Mattingly TW, Manion WC, Jahnke EJ, Nonpenetrating Traumatic Injury of the Aorta, Circulation, 17, 1086-1101, 1958.
[6] Yilmaz O, Endovascular Treatment of Traumatic Thoracic Aortic Aneurysms: Report of Five Cases and Review of the Literature, Turkish Journal of Trauma and Emergency Surgery, 16, 575-578, 2010.
[7] Kirsh MM, The Treatment of Acute Traumatic Rupture of the Aorta: a 10-year Experience, Ann Surg, 184, 308-16, 1976.
[8] Prêtre R, Blunt Injury to the Ascending Aorta: Three Patterns of Presentation, Surgery, 119, 603-609, 1996.

[9] Oppenheim, Gibt es eine Spontanruptur des gesunden Aorta und wie kommt es zustande? Mflnchen Med Wochenschrift, 65, 1234-7, 1918.
[10] Okamoto RJ, Wagenseil JE, DeLong WR, Peterson SJ, Kouchoukos NT, Sundt 3rd TM, Mechanical properties of dilated human ascending aorta, Ann Biomed Eng 30, 624-35, 2002.
[11] Choudhury N, Local mechanical and structural properties of healthy and diseased human ascending aorta tissue, Cardiovasc Pathol, 18, 83-91, 2009.
[12] Fung YC, Biomechanics: mechanical properties of living tissues. Springer, New York, 1993.
[13] Holzapfel G, Ogden R, Constitutive modelling of arteries. Proc. R. Soc. A 466, 1551–1597, 2010.
[14] Humphrey J, Cardiovascular Solid Mechanics, Springer, New York, 2002.
[15] Gasser T, Ogden R, Holzapfel G. Hyperelastic modelling of arterial layers with distributed collagen fibre orientations. J R Soc Interface 3, 15–35, 2006.
[16] Ferruzzi J, Vorp DA, Humphrey JD, On constitutive descriptors of the biaxial mechanical behavior of human abdominal aorta and aneurysms, J. R. Soc. Interface 8, 435–450, 2011.
[17] Bonow RO, ACC/AHA 2006 Guidelines for the Management of Patients with Valvular Heart Disease, Circulation, 114, e84-e231, 2006.
[18] Vahanian A, Guidelines on the Management of Valvular Heart Disease, The Task Force on the Management of Valvular Heart Disease of the European Society of Cardiology, European Heart Journal, 28, 230-268, 2007.
[19] Nicholls SC, Gardner JB, Meissner MH, Johansen KH, Rupture in Small Abdominal Aortic Aneurysms, J Vasc Surg, 28, 884-8, 1998.
[20] Pape LA, Aortic Diameter >5.5 cm Is Not a Good Predictor of Type A Aortic Dissection: Observations From the International Registry of Acute Aortic Dissection (IRAD), Circulation, 116, 1120-1127, 2007.
[21] Elefteriades JA, Farkas EA, Thoracic Aortic Aneurysm: Clinically Pertinent Controversies and Uncertainties, J Am Coll Cardiol, 55, 841-857, 2010.
[22] Vorp DA, Raghavan ML, Webster MW, Mechanical wall stress in abdominal aortic aneurysm: influence of diameter and asymmetry, J Vasc Surg, 27, 632-639, 1998.
[23] Adham M, Mechanical Characteristics of Fresh and Frozen Human Descending Thoracic Aorta, Journal of Surgical Reaserch, 64, 32-34, 1996.
[24] Holzapfel G, Gasser T, Ogden R, A New Constitutive Framework for Arterial Wall Mechanics and a Comparative Study of Material Models. J Elast, 61, 1–48, 2000.
[25] Zhang D, Eggleton C, Arola D, Evaluating the Mechanical Behavior of Arterial Tissue using Digital Image Correlation, Exp Mech, 42, 409–416, 2002.
[26] Mohan D, Melvin J, Failure properties of passive human aortic tissue. II-Biaxial tension tests, J Biomech, 16, 31–44, 1983.
[27] GOM Optical Measurement Techniques. [http://www.gom.com/metrology-systems/system-overview/aramis.html] Accessed Jan 11, 2011.
[28] Raghavan ML, Webster MW, Vorp DA, Ex vivo biomechanical behaviour of abdominal aortic aneurysms: assessment using a new mathematical model, Annals of Biomedical Engineering, 24, 573-582, 1996.
[29] Avril S, Badel P, Duprey A, Anisotropic and Hyperelastic Identification of in vitro Human Arteries From Full-Field Measurements, J Biomech, 43, 2978–2985, 2010.
[30] Kim JH, Avril S, Duprey A, Favre JP, Experimental Characterization of Rupture in Human Aortic Aneurysms using a Full-Field Measurements Technique, J Biomech Model Mechanobiol, 2012, in press.
[31] Haskett D, Johnson G, Zhou A, Utzinger U, Vande Geest J, Microstructural and Biomechanical Alterations of the Human Aorta as a Function of Age and Location, J Biomech Model Mechanobiol, 9, 725-736, 2010.